Desalination and Water Treatment
www.deswater.com

doi: 10.5004/dwt.2022.28915

274 (2022) 206–218
October

Ethylenediamine functionalized chelating resin for removal of Cu(II) and Cd(II) from aqueous solution

Youning Chen[a,*], Shuang Jia[a], Wei Zhao[a], Juan Song[b], Yuhong Li[a], Huan Wang[a]

[a]*College of Chemistry and Chemical Engineering, Xianyang Normal University, Xianyang 712000, China, emails: cyn5363@163.com. (Y.N. Chen), 2477752442@qq.com (S. Jia), xysyzw@126.com (W. Zhao), 309943006@qq.com (Y.H. Li), 237463169@qq.com (H. Wang)*
[b]*Jiangsu Key Laboratory of Chiral Pharmaceuticals Biomanufacturing, College of Pharmacy and Chemistry & Chemical Engineering, Taizhou University, Taizhou 225300, China, email: 1982558540@qq.com*

Received 15 May 2022; Accepted 4 September 2022

ABSTRACT

A novel ethylenediamine chelating resin (PEDA-*g*-PS) was prepared by grafting poly(glycidyl methacrylate) onto the chloromethylated polystyrene beads via surface-initiated atom transfer radical polymerization (SI-ATRP), and followed by the ring-opening reaction of epoxy and amine groups. The resin was characterized by infrared spectroscopy, scanning electron microscopy and elemental analysis. The adsorption property for Cu(II) and Cd(II) on the resin was examined. By analyzing adsorption isotherm, adsorption kinetics and the influence of solution pH on the adsorption capacity, the adsorption of Cu(II) and Cd(II) on PEDA-*g*-PS resin was proved to be Langmuir single-layer adsorption model, and adsorption process conformed to pseudo-second-order kinetic equation. The maximum adsorption capacities for Cu(II) and Cd(II) could reach 1.19 and 1.95 mmol·g^{-1} at pH 3.0 by fitting Langmuir model. The adsorption of the Cu(II) and Cd(II) was hardly affected by common coexisting ions such as Na(I), K(I), Ca(II) and Mg(II), whereas they were slightly decreased when Fe(II) and Zn(II) coexisted in the solution, which illustrated the selective adsorption of Cu(II) and Cd(II) from wastewater. After ten adsorption–desorption cycles, the adsorption capacity of the resin did not change significantly, indicating that the resin exhibited excellent adsorption properties for heavy metal ions and excellent reusability.

Keywords: Chloromethylated polystyrene bead; Atom transfer radical polymerization; Adsorption; Heavy metal ion

1. Introduction

With the development of industry, heavy metals have become a major threat to all life in the ecosystem and cause serious health problems [1,2]. Because heavy metals cannot be degraded, when the content of heavy metals in a living body accumulates to a certain amount, symptoms of damage such as physiological obstruction, developmental arrest, and even death will occur [3,4]. Copper and cadmium are common and highly toxic metals. Excessive intake of copper(II) by the human body can lead to liver and kidney damage, increased blood pressure and respiratory rate, damage to the central nervous system and cellular imbalances leading to pathogenic processes such as Alzheimer's disease, Menkes syndrome, inflammatory disease, and Wilson's disease [5,6]. Cadmium can cause liver and kidney damage, emphysema, hypertension, and testicular atrophy [7]. Therefore, the removal of heavy metal ions has attracted widespread attention [8–10]. The most common methods for removing heavy metal ions from wastewater include adsorption, precipitation, membrane filtration, and complex solvent extraction [11–14]. Among them, in terms of simplicity of design and simplicity of operation, the use of suitable adsorbents for adsorption is considered to be one of the most effective and attractive methods. Therefore, many

* Corresponding author.

studies have been conducted to promote the development of new adsorbents by functionalization of materials such as activated carbon, chelating resin, and silica gel [15–18].

In general, the surface of all solid materials possess the ability of adsorption. In fact, only porous materials with large specific surface area and corresponding activity can be used as adsorbents with obvious adsorption effect [19–21]. Ion-exchange adsorbents can effectively separate various ions, but lack selectivity [22,23]. Compared with ion-exchange adsorbents, chelating agents have stronger binding capacity and higher selectivity [24–26]. Therefore, the development of adsorbents with chelating function is an important part in adsorbent research [27–29]. The surface of the adsorbent is the phase boundary between the polymer and the external environment, and the performance of the chelating agent depends largely on its surface properties. The surfaces of most polymer are hydrophobic and chemically inert. In order to introduce functional groups on the surface of materials and endow the materials with better adsorption properties, a lot of research has been done on the surface modification of polymer materials [30,31]. The "Grafting from" method is to build a highly oriented and tightly bound "initiator self-assembled molecular layer" on the surface of the adsorbents via molecular self-assembly technology, and then small molecular monomers are grafted to the surface through living polymerization technology, which can form high density of polymer molecular brush structure on the surface of the material, so as to connect as many functional groups as possible in a limited area [32,33]. Among them, atom transfer radical polymerization (ATRP) is a new controlled radical living polymerization technology [34]. Combining ATRP technology, studying the preparation technology of the new adsorbent and the relationship between the grafting amount of the surface monomer and the adsorption capacity are of great significance for the preparation of high-performance adsorbents [35,36].

In this paper, poly(glycidyl methacrylate) were grafted on the chloromethylated polystyrene beads (CMPS) resin by ATRP technology firstly. Then, the ethylenediamine chelating resins were prepared via ring-opening reaction of amine group in ethylenediamine and the epoxy group in glycidyl methacrylate. The adsorption properties of resins for Cu(II) and Cd(II) were investigated. It is expected to provide theoretical guidance for the preparation of high-capacity adsorbents.

2. Experimental section

2.1. Reagents and instruments

Chloromethylated cross-linked styrene-divinylbenzene resins (18% Cl, particle size 0.30~0.45 mm) (Sunresin New Materials Co., Ltd., Xi'an, China), copper(I) bromide (Sinopharm, China, ≥98%); 2,2′-bipyridine (Sinopharm, China, ≥99.5%); glycidyl methacrylate (GMA) (CP, Aladdin, Shanghai, China); ethylenediamine (AR, Chengdu Kelong Chemical Reagent Factory); $Cd(NO_3)_2{\cdot}4H_2O$ (AR, Tianjin Fucheng Chemical Reagent Factory); $CuSO_4{\cdot}5H_2O$ (AR, Tianjin Fucheng Chemical Reagent Factory); All other chemicals were of analytical grade.

Fourier-transform spectrometer (TENSOR 27, Bruker, Germany) was used to determine the structure of the chelating resin. X-ray photoelectron spectroscopy (PHI-5400X, PerkinElmer, USA) was used to achieve the qualitative analysis of the surface elements. The concentrations of metal ions were measured by an atomic absorption spectrophotometry (AAS, novAA 400, Analytik Jena AG, Germany).

2.2. Preparation of adsorbents

2.2.1. SI-ATRP of glycidyl methacrylate on chloromethylated polystyrene beads

The synthesis method of poly(glycidyl methacrylate) on chloromethylated polystyrene beads (PGMA-*g*-PS) was given in [9]. GMA was grafted onto the surface of the initiator-functionalized resins via SI-ATRP. Briefly, 2,2-bipyridyl (0.5 g, 0.72 mmol), copper(I) bromide (0.05 g, 0.30 mmol) and CMPS beads (5.0 g) were placed in a reaction vessel, and the mixture was de-oxygenated by repeated vacuuming. High-purity nitrogen was introduced into the tube after each evacuation stage. Then, GMA (10 mL) and tetrahydrofuran (30 mL), deoxygenated by three cycles of freezing–vacuum–thaw, were added into the tube using a syringe under nitrogen atmosphere. The reaction was carried out with stirring at 40°C under nitrogen atmosphere. The beads were filtrated out from the reaction solution after the desired reaction time, and then immersed in 60 mL methanol/$EDTANa_2$ (1:1, v/v) solution for 24 h to remove copper. Finally, the resulting glycidyl methacrylate modified PS (PGMA-*g*-PS) was washed by water and methanol and dried at 35°C under vacuum for the next reaction.

2.2.2. Preparation of PEDA-g-PS

5.0 g of the modified PGMA-*g*-PS beads, 5.0 g of EDA, and 50 mL of tetrahydrofuran were added to a three-necked flask under stirring at 50°C for 8 h. The resulting PEDA-*g*-PS beads were filtered and washed thoroughly with ethanol and deionized water in sequence, and finally dried at 35°C in a vacuum oven.

2.3. Characterization

Chemical composition information about the surface of CMPS, PGMA-*g*-PS and PEDA-*g*-PS resins was analyzed using a Tensor 27 FTIR spectrophotometer (Bruker Company, Germany) and scanning electron microscope (SEM, Hitachi, Japan). A specific surface area and pore size analyzer (TriStar II 3020, Micromeritics Instrument Corporation, USA) was used to measure the Brunauer–Emmett–Teller (BET) surface area and average pore diameter.

2.4. Adsorption experiment

2.4.1. Effect of pH

0.100 g of PEDA-*g*-PS was added into a series of 100 mL of 4.0 $mmol{\cdot}L^{-1}$ metal ion solutions with different pH values from 1.0 to 7.0 (HCl, NaOH and NaAc-HAc buffer solution were used to adjust pH), and the mixtures were shaken at 200 rpm for 12 h at 25°C. The PEDA-*g*-PS was removed by filtration, and the filtrates were collected to measure the final concentration of metal ion by atomic adsorption

spectrometry. The amount of metal ion adsorbed was calculated according to Eq. (1):

$$Q_e = \frac{(C_0 - C_e)V}{W} \quad (1)$$

where Q_e is the equilibrium adsorption capacity (mmol·g^{-1}), C_0 and C_e are the initial and equilibrium metal ion concentrations (mmol·L^{-1}), respectively; V is the solution volume (L), and W is the mass of the dried resins (g).

2.4.2. Adsorption isotherms

The adsorption capacities of PEDA-*g*-PS at 25°C were measured with the following procedure. Cu(II) and Cd(II) stock solutions were adjusted to pH 3.0 and then diluted with NaAc-HAc solution (pH 3.0) to obtain a series of working solutions with different concentrations (0.2~5.0 mmol·L^{-1}). In addition, 0.1 g of PEDA-*g*-PS was added into 100.00 mL of operational solution and then shaken on a shaker for 12 h. Adsorption isotherms were obtained by plotting Q_e vs. C_e. The change of adsorption capacity with temperature was measured at 25°C, 35°C and 45°C.

2.4.3. Adsorption kinetics

To a series of 0.1 g of PEDA-*g*-PS, 100.00 mL of 4.0 mmol·L^{-1} Cu(II) and Cd(II) working solutions were added separately in vessels, and then the solutions were shaken on a shaker at 25°C. Aliquots of 1.00 mL solution were taken at different time intervals, and the concentration variations of metal ions were analyzed using AAS. The kinetic curve was obtained by plot of Q_e vs. t.

2.4.4. Selective adsorption

A series of binary mixed solutions were obtained by mixing Cu(II) and Cd(II) ions (4.0 mmol·L^{-1}) with the coexisting ions such as Na(I), K(I), Ca(II), Mg(II), Fe(III) and Zn(II) (8.0 mmol·L^{-1}) respectively. The mixture of 0.1 g of PEDA-*g*-PS resin and 100 mL of each binary mixture was shaken for 12 h at 25°C. The selectivity factor can be calculated from the adsorption capacity of metal ions in binary mixtures.

2.4.5. Competitive adsorption

The competitive adsorption among Cu(II) and Cd(II) was examined in a binary system at pH 3.0. (1) The concentration of Cu(II) was fixed at 4 mmol·L^{-1}, and the concentration of Cd(II) was controlled at 0.2~5.0 mmol·L^{-1} respectively. (2) The concentration of Cd(II) was fixed at 4 mmol·L^{-1}, and the concentration of Cu(II) was controlled at 0.2~5.0 mmol·L^{-1}, respectively. In addition, 0.1 g of PEDA-*g*-PS was added into 100.00 mL of operational solution and then shaken on a shaker for 12 h at 25°C.

2.4.6. Recycling experiments

The Cu(II)-loaded and Cd(II)-loaded PEDA-*g*-PS were put into 1.0 mol·L^{-1} HCl solution, stirred at room temperature for 5 h for desorption. The desorbed resin was collected by filtration, washed with distilled water, and reused in the next cycle of adsorption experiments.

2.5. Stability experiments

The stability of PEDA-*g*-PS resin was tested with a dissolution experiment. Two portions of 2.000 g resins were immersed into 1,000 mL 0.2 mol·L^{-1} HCl and 0.2 mol·L^{-1} NaOH solutions, separately, for one month. Then, the mixture was filtered. The filtrates were extracted using 50.0 mL ethyl acetate for three times, and the combined extract was concentrated to 5.0 mL and analyzed by gas chromatography-mass spectrometry (GC/MS) (GC7980-MS5975, Agilent Technologies, Santa Clara, CA). Samples were injected in split less mode onto a DB-5 MS column (30 m × 250 m × 0.25 m, Agilent Technologies, Santa Clara, CA). Data were processed using Agilent Technologies MSD ChemStation (version E.02). The treated PEDA-*g*-PS beads was washed with distilled water and dried for mass and elemental analysis.

3. Results and discussion

3.1. Preparation of PEDA-g-PS

The synthetic route of PEDA-*g*-PS is shown in Fig. 1.

In the first step, poly(glycidyl methacrylate) (PGMA) was grafted onto the surface of chloromethylated polystyrene (PS) beads by SI-ATRP. The effect of the monomer concentration and the reaction time on the degree of grafting are indicated in [9]. In the second-step, ethylenediamine chelating resin was prepared by the ring-opening reaction of epoxy and amine groups.

3.2. Characterization of resin

Fourier-transform infrared (FTIR) spectra of CMPS, PGMA-*g*-PS and PEDA-*g*-PS resins are shown in Fig. 2. It can be seen from Fig. 2a that the characteristic absorption peaks at 2,934 and 1,460 cm^{-1} represent the stretching vibration and skeleton vibration of –CH_2– in the aromatic ring, respectively. The absorption peaks at 759 and 698 cm^{-1} are the stretching vibrations of C–Cl in –CH_2Cl [9]. After the surface modification of the resin, the characteristic absorption peaks in Fig. 2b and c changed significantly. In Fig. 2b, a strong absorption peak appears at 1,723 cm^{-1}, which is the stretching vibration peak of C=O in GMA. 1,243 and 1,145 cm^{-1} are the symmetrical and asymmetrical vibrational absorption peaks of C–O in GMA. There appears to be characteristic absorption peaks of epoxy groups at 907 and 841 cm^{-1} in the PGMA-*g*-PS resin, suggesting the successful grafting of GMA [37]. After the ring-opening reaction of ethylenediamine and epoxy group, the absorption peaks at 907 and 841 cm^{-1} disappeared (Fig. 2c). A broad peak appeared at 3,100–3,700 cm^{-1}, corresponding to the combination of –OH and –NH stretching vibrations, indicating that –OH and –NH were introduced to the resin surface. A new absorption peak appeared at 1,570 cm^{-1}, which belongs to the deformation vibration of –NH, further confirming successful introduction of amine groups onto the resin surface.

X-ray photoelectron spectroscopy (XPS) was also used to analyze the surface composition and the changes in

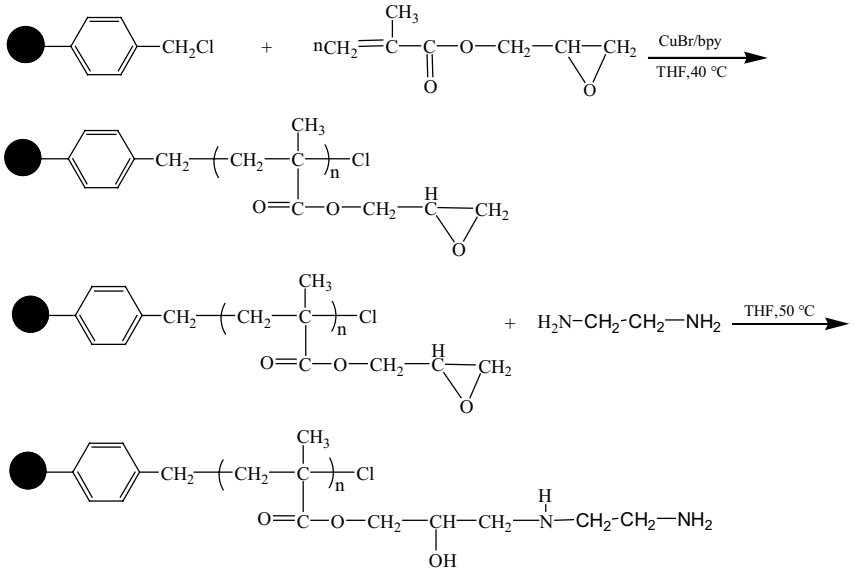

Fig. 1. Synthetic route for the preparation of PEDA-*g*-PS.

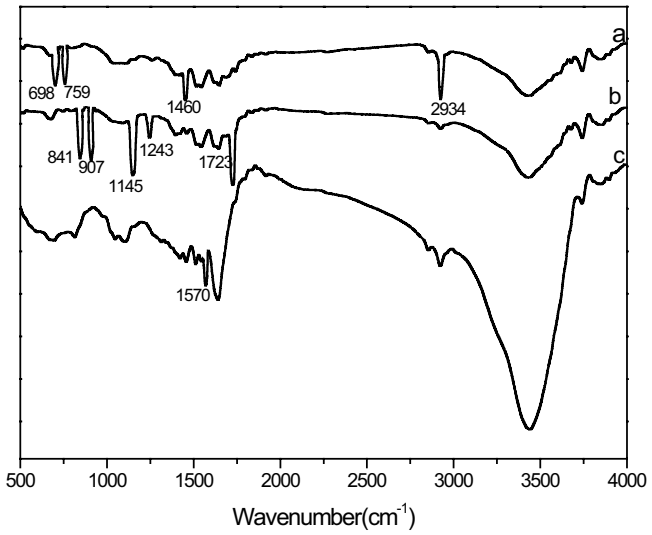

Fig. 2. FTIR spectrum of (a) CMPS, (b) PGMA-*g*-PS and (c) PEDA-*g*-PS resins.

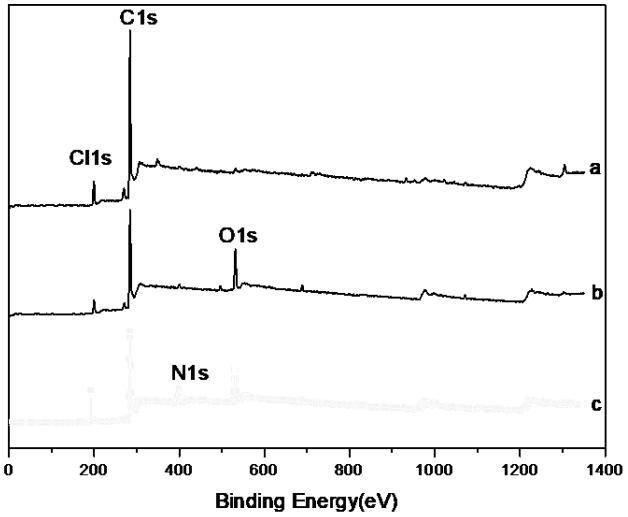

Fig. 3. XPS wide scan of (a) CMPS, (b) PGMA-*g*-PS and (c) PEDA-*g*-PS resins.

functional groups of the resin of CMPS, PGMA-*g*-PS and PEDA-*g*-PS resins. Fig. 3 shows the XPS wide scan of the resin before and after the modification. As seen from Fig. 3c, the N1s peak appeared at 398.1 eV, indicating that amino group was successfully introduced into the resins through the amination reaction. C1s core-level spectra of PEDA-*g*-PS resins were investigated. As shown in Fig. 4, four peaks appeared at 283.5, 284.1, 284.9 and 285.8 eV, which corresponded to C–C, C–N, C–Cl/C–O and C=O, respectively.

The results of elemental analysis and pore structure parameters of resins are shown in Table 1. It can be seen that the element content of the resin surface changed significantly before and after modification. For PEDA-*g*-PS resin, the N content increased significantly, indicating that the ring-opening reaction had occurred on the resin surface, and amine groups were successfully introduced onto the resin surface. The physical structure of the resins was characterized by N_2 adsorption–desorption isotherms. The obtained porous structure parameters of the resins are summarized in Table 1. The surface area, average pore diameter and Barrett–Joyner–Halenda (BJH) cumulative volume of PEDA-*g*-PS were all smaller than those of CMPS. It may be because some macropores are filled during the synthesis reaction, which causes these parameters to become smaller than before modification.

Fig. 5 shows the SEM images of CMPS, PGMA-*g*-PS and PEDA-*g*-PS resins. It can be seen that the surface of the CMPS resin was relatively smooth (Fig. 5a), indicating that there were very few branches in the CMPS resin and therefore its adsorption performance was poor. After modification,

the surface of the resin became rough (Fig. 5b and c), indicating that the resin surface was successfully grafted with amine groups.

All these results confirmed the successful grafting of PGMA and the introduction of the amine groups on the surface of the resin.

3.3. Adsorption property for heavy metal ions

3.3.1. Effect of pH on adsorption

As shown in Fig. 6, the effect of solution pH on the adsorption capacity were studied. In order to avoid the formation of hydroxide precipitation, the adsorption for Cu(II) and Cd(II) was carried out at pH 7.0 or lower. It can be seen from Fig. 6 that the adsorption capacity of the resin for the two ions were increased with the increasement of pH. At lower pH, the adsorption capacity was small. This was because the amine group was positively charged with protonation at lower pH, which prevented the metal cations from approaching the adsorption site due to electrostatic repulsion. With the increase of pH, the amine groups on the

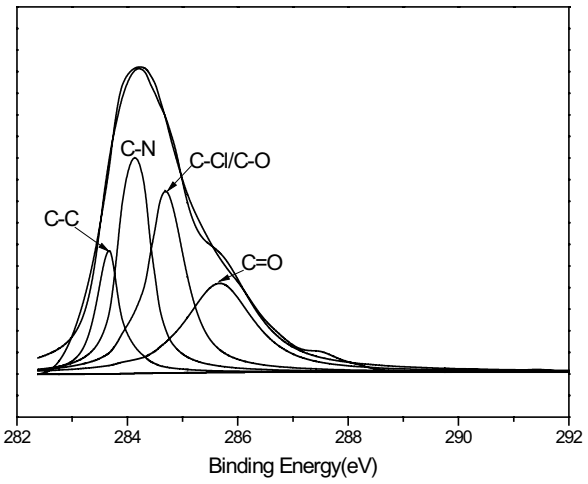

Fig. 4. C1s core-level spectra of PEDA-*g*-PS resins.

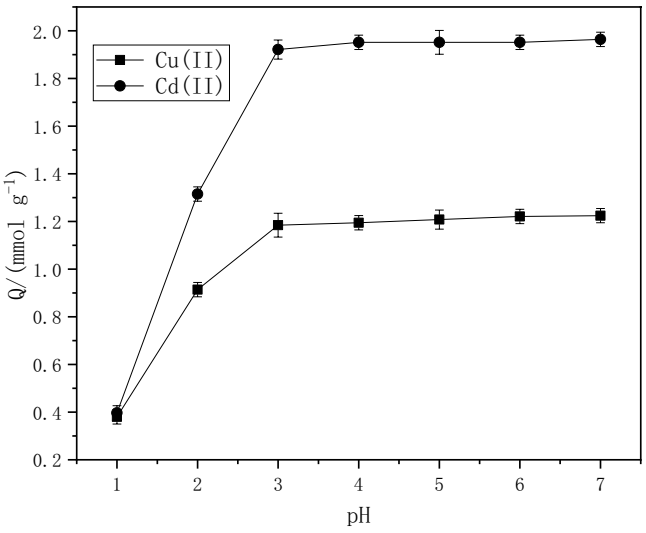

Fig. 6. Effect of pH on the adsorption of PEDA-*g*-PS resin for Cu(II) and Cd(II) (initial concentration: 4 mmol·L^{-1}; 25°C; adsorbent dose: 0.1 g).

Table 1
Elemental analysis and pore structure parameters

Sample	Element content (%)			Pore structure parameters		
	C	H	N	BET surface area ($m^2 \cdot g^{-1}$)	BJH cumulative volume ($cm^3 \cdot g^{-1}$)	Average pore diameter (nm)
CMPS	56.67	8.690	0.455	28.81	0.20	19.71
PGMA-*g*-PS	72.48	5.186	0.004	22.08	0.17	16.56
PEDA-*g*-PS	70.98	7.045	12.23	19.69	0.14	12.48

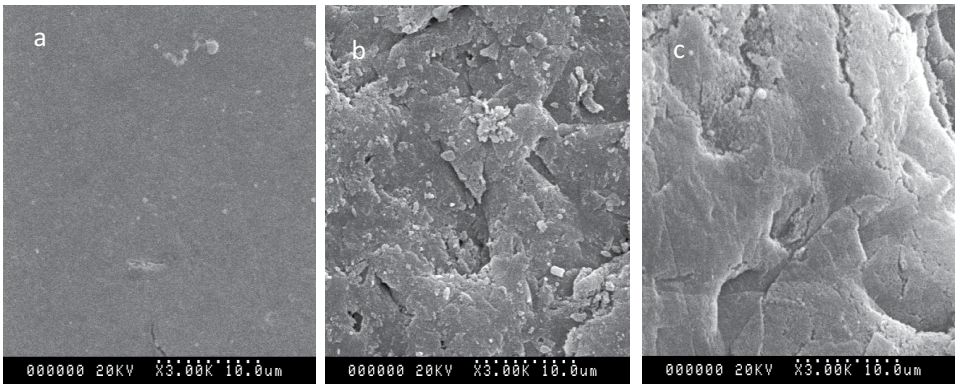

Fig. 5. SEM surface images of the resins of (a) CMPS, (b) PGMA-*g*-PS and (c) PEDA-*g*-PS resins.

resin surface were chelated with Cu(II) and Cd(II) to produce adsorption.

3.3.2. Effect of adsorbent dosage

The adsorbent dosage is an important parameter in adsorption studies because it determines the capacity of adsorbent for a given initial concentration of absorbate solution. To study the dosage effect of the PEDA-*g*-PS resin on Cu(II) and Cd(II) adsorption, experiments were conducted at initial metal ion concentration of 4.0 mmol·L^{-1} (pH 3.0), while the amount of PEDA-*g*-PS resin added was varied. Fig. 7 shows the effect of adsorbent dosage on the adsorption capacity of Cu(II) and Cd(II). It was observed that the adsorption capacity of heavy metal ions rapidly increased with the increase in adsorbent dosage up to 0.1 g, and thereafter remained unchanged. The adsorption capacity increase at lower adsorbent dosage was due to the increase in the available sorption sites on the surface of PEDA-*g*-PS resin.

3.3.3. Adsorption isotherms

The adsorption isotherm is usually used to evaluate the adsorption capacity of the adsorbent. The adsorption isotherm of Cu(II) and Cd(II) at 25°C by the resin is shown in Fig. 8.

Langmuir (2) and Freundlich (3) adsorption isotherm models are often used to describe the adsorption equilibrium of liquid–solid systems [38].

$$\frac{C_e}{Q_e} = \frac{1}{Q_0 K_C} + \left(\frac{1}{Q_0}\right) C_e \tag{2}$$

$$\ln Q_e = \ln K_F + \frac{1}{n} \ln C_e \tag{3}$$

where Q_e is the adsorption capacity, mmol·g^{-1}; C_e is the equilibrium concentration of metal ions, mmol·L^{-1}; Q_0 is the saturated adsorption capacity, mmol·g^{-1}; K_C is the Langmuir adsorption constant; K_F is an empirical parameter; n is the Freundlich constant.

The Langmuir model is based on the assumption of surface homogeneity such as equally available adsorption, monolayer surface coverage, and no interaction between adsorbed species, whereas the Freundlich model assumes that the adsorption occurs on a heterogeneous surface. The results are shown in Table 2. When comparing the R^2 values for the applied Freundlich and Langmuir models, we see that Langmuir equation represented a better fit to the experimental data than the Freundlich equation in all cases for the adsorption of metal ions. This reflects that the surface of the resin was made up of small homogeneous adsorption patches.

3.3.4. Adsorption kinetics

The adsorption process of the adsorbent on the porous adsorbent usually includes external diffusion, internal particle diffusion and active site adsorption, while intraparticle diffusion plays an important role in the kinetics of adsorption [39]. Fig. 9 shows the adsorption kinetics curves for Cu(II) and Cd(II) of the resin. The adsorption equilibrium was reached at 2.5 h and 4 h for Cu(II) and Cd(II), respectively.

In order to study the kinetic mechanism of adsorption process, three different kinetic models proposed by Weber and Morris [30], pseudo-second-order kinetic model (3), Lagergren's pseudo-first-order kinetic model (4), and intraparticle diffusion model (5), were used to explain the kinetic process.

$$\frac{t}{Q_t} = \frac{1}{kQ_e^2} + \frac{1}{Q_e} t \tag{3}$$

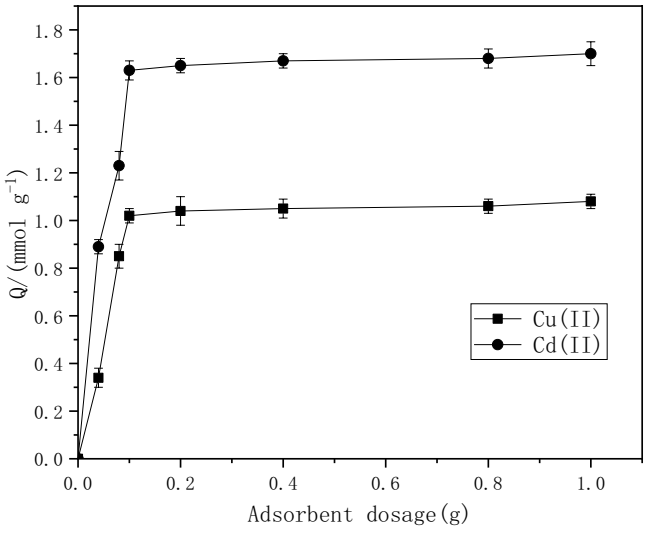

Fig. 7. Effect of adsorbent dosage on the adsorption of PEDA-*g*-PS resin for Cu(II) and Cd(II) (initial concentration: 4.0 mmol·L^{-1}; 25°C; pH 3.0).

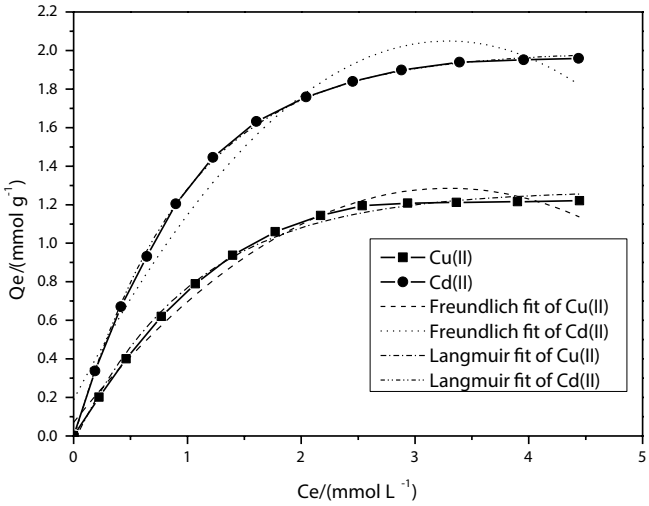

Fig. 8. Adsorption isotherms of PEDA-*g*-PS resin for Cu(II) and Cd(II) at 25°C (pH 3.0; contact time: 12 h; adsorbent dose: 0.1 g).

Table 2
Parameters obtain by Langmuir and Freundlich for the adsorption of Cu(II) and Cd(II) on PEDA-*g*-PS resins at 25°C

Ion metals	Experimentally determined Q_e (mmol·g^{-1})	Langmuir parameter			Freundlich parameter		
		Q_0 (mmol·g^{-1})	K_C	R_L^2	K_F	$1/n$	R_F^2
Cu(II)	1.02	1.19	35.58	0.98611	0.482	0.657	0.96982
Cd(II)	1.63	1.95	45.76	0.99236	0.731	0.614	0.97547

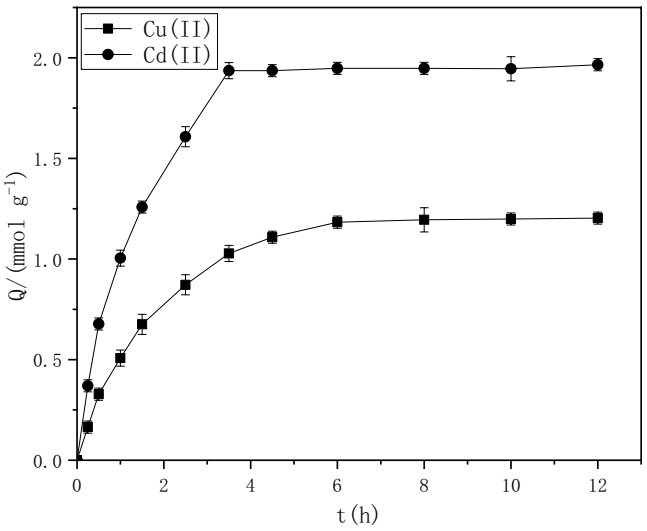

Fig. 9. Adsorption kinetics of PEDA-*g*-PS resin for Cu(II) and Cd(II) (initial concentration: 4 mmol·L^{-1}; 25°C; pH 3.0; adsorbent dose: 0.1 g).

$$\lg\left(Q_e - Q_t\right) = \lg Q_e + \frac{k_{ads}}{2.303}t \quad (4)$$

$$Q_t = k_{id}t^{0.5} \quad (5)$$

Table 3
First-order and second-order rate constants

Equations	Parameters	Cu(II)	Cd(II)
Pseudo-first-order kinetic equation	Q_e (mmol·g^{-1})	1.28	2.02
	k_{ads} (1/h)	0.241	0.389
	R^2	0.8851	0.8732
Pseudo-second-order kinetics	Q_e (mmol·g^{-1})	1.40	2.16
	k (g·mmol^{-1}·h^{-1})	0.472	0.581
	R^2	0.9946	0.9945
Intraparticle diffusion equation	K_{id} (mmol·g^{-1}·h$^{-1/2}$)	0.198	0.296
	R^2	0.962	0.971

where t is the adsorption time (min); k the adsorption rate constant (min^{-1}); k_{ads} is the Lagergren rate constant (min^{-1}) of the adsorption; K_{id} is the intraparticle diffusion rate constant (mmol·g^{-1}·min$^{-0.5}$), and Q_t and Q_e are the adsorption amount at given time t and equilibrium time, respectively.

The kinetic fitting curve is shown in Fig. 10 and the fitting results are listed in Table 3. Obviously, as it can be seen from Fig. 10 and Table 3, R^2 values of the pseudo-second-order kinetic were higher than the pseudo-first-order kinetics. Therefore, the adsorption behavior for Cu(II) and Cd(II) of PEDA-*g*-PS resin followed the pseudo-second-order kinetic model.

According to Weber and Morris, an adsorption process is divided into three steps: (1) diffusion of the

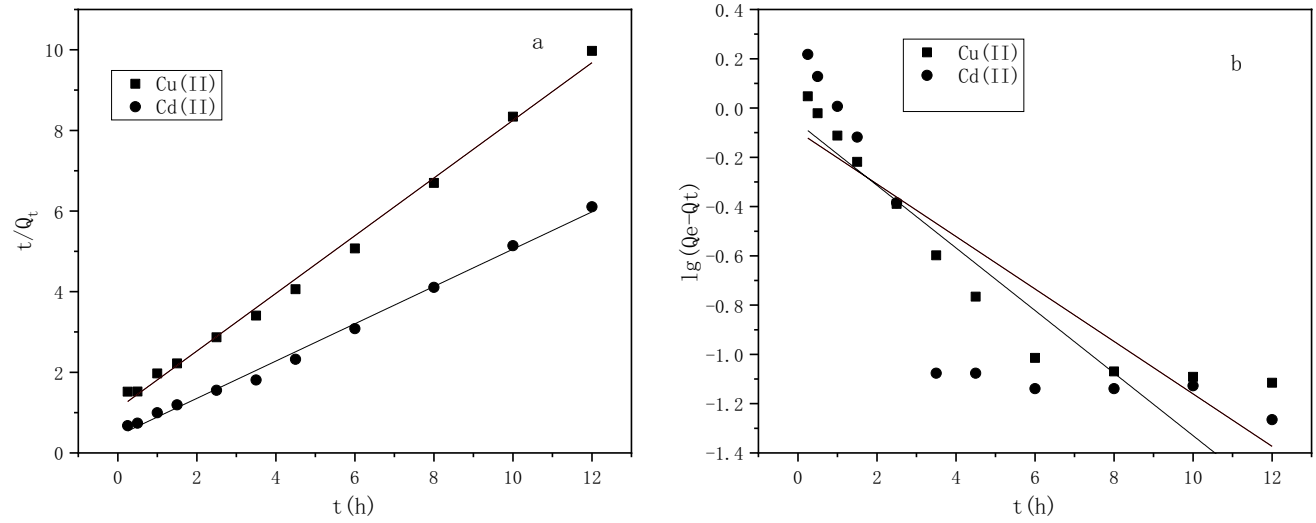

Fig. 10. Kinetic fitting curve (a) pseudo-second-order model and (b) pseudo-first-order model.

adsorbate from the solution to the surface of the adsorbent; (2) internal diffusion process, usually determined by the pore size of the adsorbent; (3) adsorption of the adsorbate with the surface active sites in the adsorbent.

According to Eq. (5), if the curve gives a straight line, internal diffusion can be accepted as the only rate limiting step, but multiple linearity's are formed, indicating that two or more stages are involved in metal ion adsorption [31]. As shown in Fig. 11, the adsorption process is divided into three stages: (1) rapid transport of metal ions from solution to the surface of the resin (2) gradual adsorption stage, where intraparticle diffusion is the rate limiting step, and (3) final equilibrium stage, intraparticle diffusion begins to slow down because the concentration of metal ions in the solution is very low and the number of available adsorption sites is small.

From the above analysis, it can be seen that intraparticle diffusion was not the only rate-controlling step, indicating that the adsorption process involved several single kinetic stages.

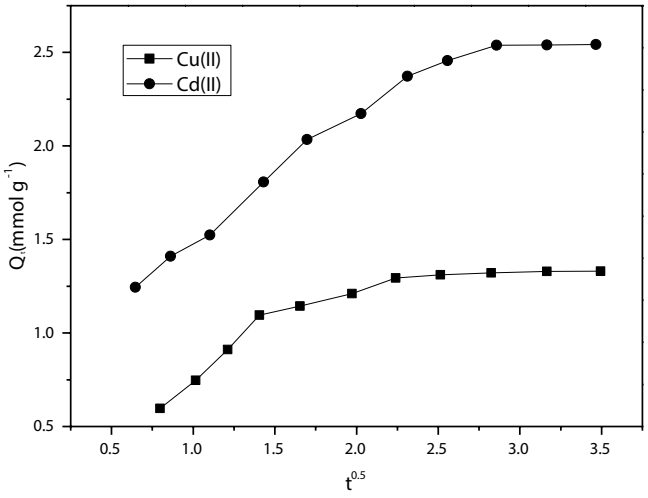

Fig. 11. Plot of Weber–Morris intraparticle diffusion model for the adsorption of metal ions on PEDA-*g*-PS resin.

3.3.5. Adsorption thermodynamics

The adsorption capacity of Cu(II) and Cd(II) on PEDA-*g*-PS resins were increased with the increasing of temperature, but the increasement was not significant in the temperature range investigated (Fig. 12), which confirmed that the adsorption was an endothermic process.

The thermodynamic parameters provide insight information of inherent energetic changes associated with adsorption, including free energy change (ΔG), enthalpy change (ΔH) and entropy change (ΔS), which can be respectively estimated using the following equations [40]:

$$\Delta G = -RT\ln K_C \tag{6}$$

$$\ln K_C = \frac{-\Delta H}{RT} + \frac{\Delta S}{R} \tag{7}$$

where R is the universal gas constant (8.314 J·mol^{-1}·K^{-1}), T the absolute temperature (K), and K_C the adsorption equilibrium constant, which was obtained from the Langmuir isotherm at different temperatures.

Using a linear plot between lnK_C vs. 1/T, the adsorption enthalpy and entropy for the adsorption process of the ions could be obtained according to the slope and intercept of the plot, as shown in Table 4.

The negative value of ΔG indicated that the adsorption process of PEDA-*g*-PS resin on metal ions were spontaneous. The positive values of ΔH and ΔS for the adsorption of the two ions demonstrated an endothermic nature for this process along with an increased randomness at the solid/liquid interface, indicating that the temperature was a beneficial factor in the adsorption kinetics.

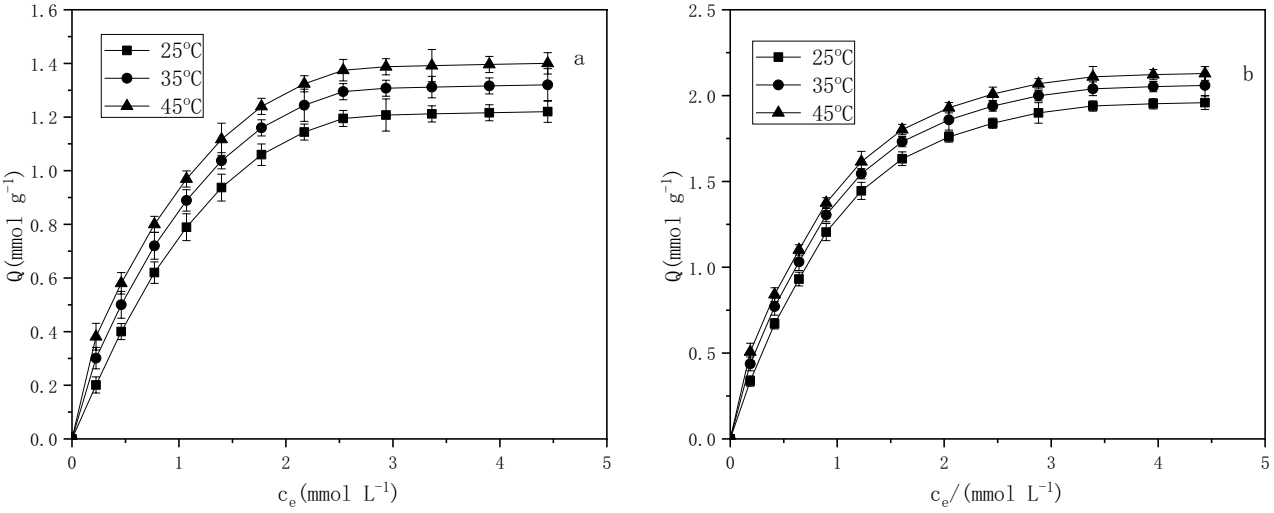

Fig. 12. Adsorption isotherms of PEDA-*g*-PS resin for (a) Cu(II) and (b) Cd(II) at different temperature (pH 3.0; contact time: 12 h; adsorbent dose: 0.1 g).

3.3.6. Selective adsorption

The effects of Na(I), K(I), Ca(II), Mg(II), Fe(III) and Zn(II) on the adsorption of Cu(II) and Cd(II) on PEDA-*g*-PS were investigated. As shown in Table 5, the influences of Na(I), K(I), Ca(II) and Mg(II) on the adsorption of Cu(II) and Cd(II) can be ignored, but Fe(III) and Zn(II) displayed a minor influence. However, PEDA-*g*-PS preferred adsorbing Cu(II) and Cd(II) rather than Fe(III) and Zn(II). According to the obtained results, the amine group had the property of soft base. Correspondingly, compared with Na(I), K(I), Ca(II), Mg(II) (hard acid), Fe(III) and Zn(II) were more easily combined with soft base, which affected the adsorption of Cu(II) and Cd(II) by the resin. These results illustrated that the resin could selectively adsorb Cu(II) and Cd(II) from wastewater.

3.3.7. Competitive adsorption

A competitive adsorption experiment among Cu(II) and Cd(II) was examined in a binary system. The concentration of Cd(II) in the mixed solution was fixed, the concentration of Cu(II) was changed, and the isothermal adsorption of Cu(II) was observed as shown in Fig. 13a. Similarly, as shown in Fig. 13b, the concentration of Cu(II) in the mixed solution was fixed, the concentration of Cd(II) was changed, and the isothermal adsorption of Cd(II) was observed. The adsorption capacity for Cu(II) and Cd(II) by PEDA-*g*-PS resin in binary system was lower than that in single system. Due to the presence of Cd(II), the adsorption of Cu(II) by PEDA-*g*-PS resin decreased significantly. The presence of Cu(II) also influenced the adsorption of PEDA-*g*-PS resin for Cd(II). After adding competing ions, although the adsorption isotherm of Cu(II) and Cd(II) dropped significantly, it basically kept the original shape, which indicated that the adsorption of Cu(II) and Cd(II) on the resin still obeyed the isotherm adsorption model after adding competing ions. Table 6 shows the fitting parameter of Langmuir model. From Table 6 it can be seen that the saturated adsorption of Cu(II) decreased by 30.3% due to the presence of competing ions, while that of Cd(II) decreased by 16.4%, indicating that the presence of Cd(II) has a greater impact on the adsorption of Cu(II), probably because Cd(II) can coordinate with the hydroxyl and amine groups in the PEDA-*g*-PS resin.

3.3.8. Reusability of PEDA-g-PS resin

When the resin was desorbed with 0.1 mmol·L^{-1} HCl solution, the desorption rate reached 95.8%. In order to demonstrate the reusability of the adsorbent, an

Table 4
Thermodynamic parameters estimated for adsorption of two metal ions on PEDA-*g*-PS resins

Metal ions	ΔH (kJ·mol^{-1})	ΔS (J·mol^{-1}·K^{-1})	ΔG (kJ·mol^{-1})		
			25°C	35°C	45°C
Cu(II)	6.21	50.50	–8.849	–9.339	–9.859
Cd(II)	11.25	69.50	–9.473	–10.153	–10.863

Table 5
Effect of coexisting metal ions on the adsorption capacity of Cu(II) and Cd(II) (pH 3.0; contact time: 12 h; adsorbent dose: 0.1 g)

Coexisting ions	Selective coefficients	
	Cu(II)	Cd(II)
K(I)	∞	∞
Na(I)	∞	∞
Ca(II)	∞	∞
Mg(II)	∞	∞
Fe(III)	15.6	12.4
Zn(II)	13.2	10.8

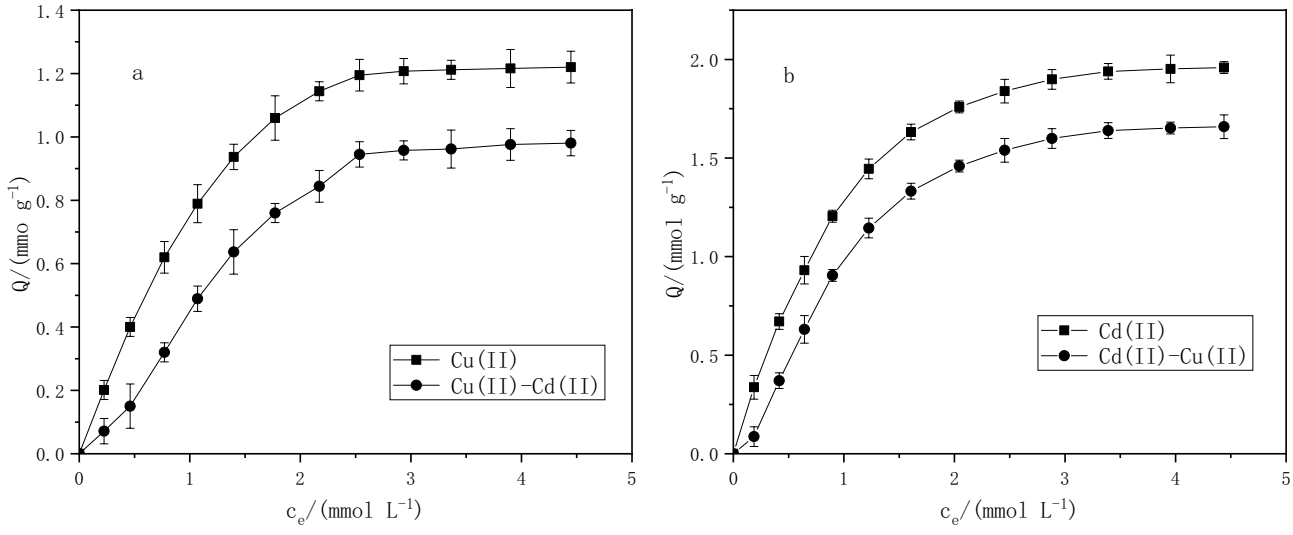

Fig. 13. Competitive adsorption of PEDA-*g*-PS resin for Cu(II) and Cd(II) (pH 3.0; contact time: 12 h; adsorbent dose: 0.1 g): (a) effect of Cd(II) on the adsorption isotherm of Cu(II) and (b) effect of Cu(II) on the adsorption isotherm of Cd(II).

adsorption–desorption cycle was repeated ten times. The results were shown in Fig. 14. After ten adsorption–desorption cycles, the adsorption capacity of the resin was reduced by only 3.21% for Cu(II) and 2.54% for Cd(II). These results indicated that PEDA-*g*-PS resin could be repeatedly used in heavy-metal adsorption without any detectable change in adsorption capacity.

3.4. Adsorption mechanism

In order to further illustrate the adsorption mechanism of PEDA-*g*-PS resins for Cu(II) and Cd(II), Fig. 15 represents the FTIR spectra of PEDA-*g*-PS resins before and after the adsorption. The results indicated that the vibration band of asymmetric vibration absorption of $–NH_2$ in PEDA-*g*-PS resins had shifted from 1,570 cm^{-1} to lower wavenumbers of 1,545 and 1,558 cm^{-1} for Cd(II) and Cu(II) adsorption, respectively. This was the result of coordination of $–NH_2$ to Cd(II) and Cu(II).

In addition, the absorption bands lying at 1,430 cm^{-1} (related to the hydroxyl group) had shifted to lower wavenumber of 1,410 cm^{-1} after adsorption for Cd(II), while for Cu(II) adsorption, these absorption bands were not far away with those before adsorption. The information implied that –OH groups had participated in the coordination with Cd(II), but had no contribution to the coordination with Cu(II), which may cause the differences in the adsorption capacity for Cd(II) and Cu(II) removal.

Table 6
Langmuir adsorption parameter of Cu(II) and Cd(II) in different ion system

Ion system	Q_0 (mmol·g^{-1})	K_C	R_L^2
Cu(II)	1.19	35.58	0.98611
Cu(II)–Cd(II)	0.83	28.52	0.9543
Cd(II)	1.95	45.76	0.99236
Cd(II)–Cu(II)	1.63	42.13	0.9654

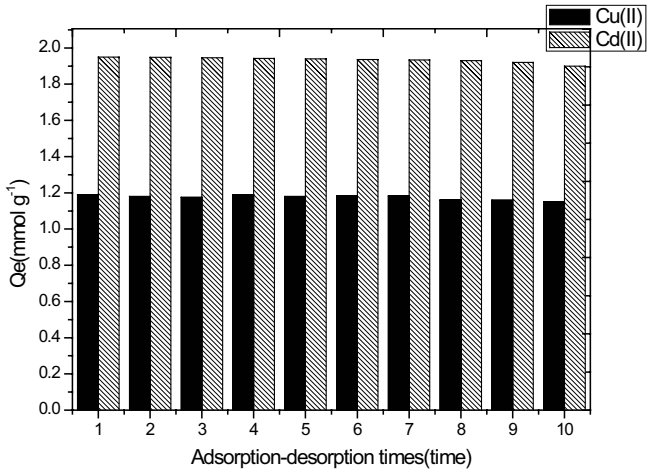

Fig. 14. Adsorption capacity of PEDA-*g*-PS resin after ten adsorption–desorption cycles (pH 3.0; initial concentration: 4 mmol·L^{-1}; contact time: 12 h; adsorbent dose: 0.1 g).

XPS analysis was performed to investigate the molecular level information of Cu(II) and Cd(II) adsorption on the PEDA-*g*-PS resins, as shown in Fig. 16. Before adsorption, the N1s and O1s binding energy locate at 398.1 eV and 533.4 eV respectively. After Cu(II) adsorption, the N1s band was shifted to 399.3 eV, due to the formation of bonds between the nitrogen and the Cu(II), while the O1s peak did not change compared with before adsorption, indicating that a complex between Cu(II) and nitrogen occurred and the adsorption of iron in the resin. After Cd(II) adsorption, the N1s and O1s band was shifted to 399.8 and 534.2 eV respectively, indicating that –OH groups have participated in the coordination with Cd(II).

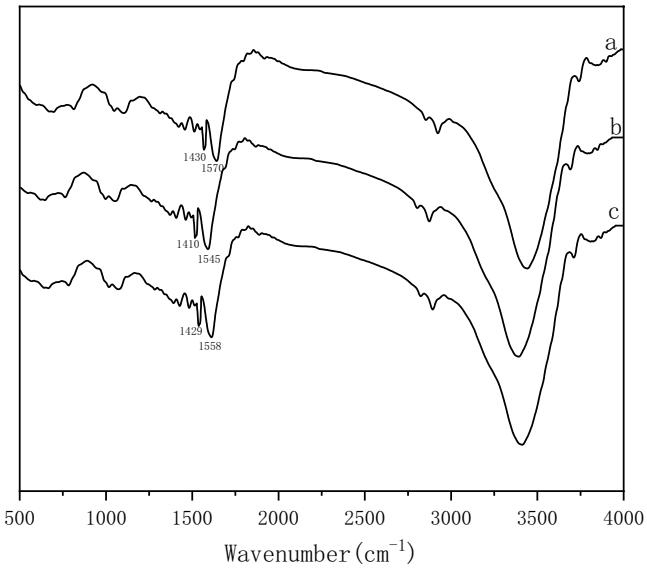

Fig. 15. FTIR spectrum of (a) PEDA-*g*-PS resins, (b) Cd(II)-loaded PEDA-*g*-PS resins and (c) Cu(II)-loaded PEDA-*g*-PS resins.

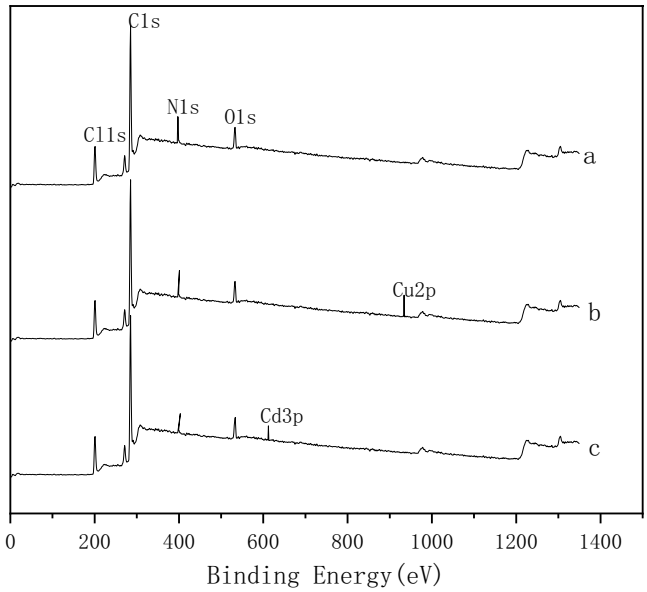

Fig. 16. XPS wide scan of (a) PEDA-*g*-PS resins, (b) Cu(II)-loaded PEDA-*g*-PS resins and (c) Cd(II)-loaded PEDA-*g*-PS resins.

Table 7
Comparison of Cu(II) and Cd(II) adsorption on PEDA-*g*-PS resins with other adsorbents

Adsorbents	Adsorption capacities (mmol·g^{-1})		Reference
	Cu(II)	Cd(II)	
Nanosized titanate composites (NaxFeyMgiTiOz)	0.22	0.079	[41]
Activated carbons	0.73	0.74	[42]
Ferromanganese binary oxide–biochar composites	1.01	0.90	[43]
Microwave-functionalized cellulose	–	1.35	[44]
β-cyclodextrin modified magnetic graphene oxide nanohybrids	0.80	–	[45]
Brazilian Orchid Tree (*Pata-de-vaca*)	0.238	0.113	[46]
PEDA-*g*-PS resin	1.19	1.95	This work

3.5. Stability of PEDA-g-PS resin

To demonstrate the stability of PEDA-*g*-PS resins, the PEDA-*g*-PS resins were immerged into strong acid and base solution for one month, respectively. No weight loss was found after treatment. The filtration solution was analyzed by GC-MS, and the ingredients of the resins, divinylbenzene, vinylbenzene and other aromatic compounds were not checked out in Compound Libraries, indicating no leakage of the harmful compounds from the materials. These results indicate that PEDA-*g*-PS resin is insoluble in aqueous solution, and the amino group in the resin has better stability in solution.

3.6. Comparison with other adsorbents

There are many adsorbents designed for different metal ions in the reference, the representative adsorbents that can adsorb Cu(II) and Cd(II) ions were chosen for comparison with PEDA-*g*-PS. As shown in Table 7, PEDA-*g*-PS beads had much higher adsorption capacities for the two metal ions than other adsorbents. Higher adsorption capacities can produce higher productivity for water treatment. Therefore, the resin should be of value in water treatment on the basis of sustainability principles.

4. Conclusions

In this work, a novel PEDA-*g*-PS resin with high capacity was prepared by SI-ATRP and ring-opening reaction. FTIR and elemental analysis confirmed the successful grafting of PGMA and the introduction of the amine groups on the surface of the resin.

The PEDA-*g*-PS resin was used to remove Cu(II) and Cd(II) from aqueous solution. The maximum adsorption of the resin for Cu(II) and Cd(II) reached 1.19 and 1.95 mmol·g^{-1} at pH 3.0 by fitting Langmuir equation. Adsorption kinetics followed the pseudo-second-order kinetic equation, and adsorption thermodynamics indicated the endothermic nature of the adsorption process. Competition from common coexisting ions, such as Na(I), K(I), Ca(II) and Mg(II), was negligible, whereas the coexisting Fe(III) and Zn(II) ions displayed only a minor influence, which illustrated the selective adsorption of Cu(II) and Cd(II) from wastewater. The resin was adsorbed–desorbed 10 times without significant change in adsorption capacity, indicating that the resin has broad application prospects in the treatment of heavy metal wastewater.

Acknowledgments

This work was supported by "Cyanine Talent" of Xianyang Normal College (No. XSYQL201710), Scientific research project of Xianyang Normal College (No. XSYK19047), Science and Technology Plan Project of Xianyang (No. 2019k02-29), Innovative Entrepreneurship Training Program for College Students; 202210722003 (No. XYSFXY2022003; 202210722003), Shaanxi Province Science and Technology Plan Project of China (No. 2021JQ-815) Shaanxi Province Science and Technology Plan Project of China (No. 2022GY-381).

References

[1] S.S. Kalaivani, A. Muthukrishnaraj, S. Sivanesan, L. Ravikumar, Novel hyperbranched polyurethane resins for the removal of heavy metal ions from aqueous solution, Process Saf. Environ. Prot., 104 (2016) 11–23.
[2] P. Bhunia, S. Chatterjee, P. Rudra, S. De, Chelating polyacrylonitrile beads for removal of lead and cadmium from wastewater, Sep. Purif. Technol., 19 (2018) 202–213.
[3] J.T. Gu, S.J. Yuan, W.T. Shu, W. Jiang, S.W. Tang, B. Liang, S.O. Pehkonen, PVBC microspheres tethered with poly(3-sulfopropyl methacrylate) brushes for effective removal of Pb(II) ions from aqueous solution, Colloids Surf., A, 498 (2016) 218–230.
[4] F.-Q. An, R.-Y. Wu, M. Li, T.-P. Hu, J.-F. Gao, Z.-G. Yuan, Adsorption of heavy metal ions by iminodiacetic acid functionalized D301 resin: kinetics, isotherms and thermodynamics, React. Funct. Polym., 118 (2017) 42–50.
[5] V. Nejadshafiee, M.R. Islami, Adsorption capacity of heavy metal ions using sultone-modified magnetic activated carbon as a bio-adsorbent, Mater. Sci. Eng., C, 101 (2019) 42–45.
[6] X. Yuan, C.C. Zhang, M.L. Xie, X. Li, Spatially ordered chelating resin based on liquid-crystal phase with highly selective removal of metal ions, Colloids Surf., A, 586 (2020) 124235, doi: 10.1016/j.colsurfa.2019.124235.
[7] G.L. Wang, R. Yang, Y.W. Liu, J.Y. Wang, W. Tan, X.S. Liu, Y. Jin, J.J. Qu, Adsorption of Cd(II) onto *Auricularia auricula* spent substrate biochar modified by CS_2: characteristics, mechanism and application in wastewater treatment, J. Cleaner Prod., 367 (2022) 132882, doi: 10.1016/j.jclepro.2022.132882.
[8] M. Medykowska, M. Wiśniewska, K. Szewczuk-Karpisz, R. Panek, Interaction mechanism of heavy metal ions with the nanostructured zeolites surface – adsorption, electrokinetic and XPS studies, J. Mol. Liq., 357 (2022) 119144, doi: 10.1016/j.molliq.2022.119144.
[9] J.C. Zhang, Y.N. Chen, Uptake of Fe(III), Ag(I), Ni(II) and Cu(II) by salicylic acid-type chelating resin prepared via

surface-initiated atom transfer radical polymerization, RSC Adv., 6 (2016) 69370–69380.
[10] S.S.G. Santos, M.B.B. Pereira, R.K.S. Almeida, A.G. Souza, M.G. Fonseca, M. Jaber, Silylation of leached-vermiculites following reaction with imidazole and copper sorption behavior, J. Hazard. Mater., 306 (2016) 406–418.
[11] A.O. Dada, F.A. Adekola, E.O. Odebunmi, F.E. Dada, O.S. Bello, A.S. Ogunlaja, Bottom-up approach synthesis of core-shell nanoscale zerovalent iron (CS-nZVI): physicochemical and spectroscopic characterization with Cu(II) ions adsorption application, MethodsX, 7 (2020) 100976, doi: 10.1016/j.mex.2020.100976.
[12] D.-Q. Cao, X. Song, X.-M. Fang, W.-Y. Yang, X.-D. Hao, E. Iritani, N. Katagiri, Membrane filtration-based recovery of extracellular polymer substances from excess sludge and analysis of their heavy metal ion adsorption properties, Chem. Eng. J., 354 (2018) 866–874.
[13] D. Iannazzo, A. Pistone, I. Ziccarelli, C. Espro, S. Galvagno, S.V. Giofré, R. Romeo, N. Cicero, G.D. Bua, G. Lanza, L. Legnani, M.A. Chiacchio, Removal of heavy metal ions from wastewaters using dendrimer-functionalized multi-walled carbon nanotubes, Environ. Sci. Pollut. Res., 24 (2017) 14735–14747.
[14] Y. Sun, Y.G. Su, Z.B. Zhao, J.X. Zhao, M. Ye, X.R. Wen, Capacitive heavy metal ion removal of 3D self-supported nitrogen-doped carbon-encapsulated titanium nitride nanorods via the synergy of faradic-reaction and electro-adsorption, Chem. Eng. J., 443 (2022) 136542, doi: 10.1016/j.cej.2022.136542.
[15] A.A. Yakout, M.A. Shaker, K.Z. Elwakeel, W. Alshitari, Response surface methodological optimization of batch Cu(II) sorption onto succinic acid functionalized SiO_2 nanoparticles, Can. J. Chem., 97 (2019) 1–10, doi: 10.1139/cjc-2018-0086.
[16] K.Z. Elwakeel, A.A. El-Bindary, E.Y. Kouta, E. Guibal, Functionalization of polyacrylonitrile/Na-Y-zeolite composite with amidoxime groups for the sorption of Cu(II), Cd(II) and Pb(II) metal ions, Chem. Eng. J., 332 (2018) 727–736.
[17] K.Z. Elwakeel, M.H. Aly, M.A. El-Howety, E. El-Fadaly, A. Al-Said, Synthesis of chitosan@activated carbon beads with abundant amino groups for capture of Cu(II) and Cd(II) from aqueous solutions, J. Polym. Environ., 26 (2018) 3590–3602.
[18] A.A. Atia, A.M. Donia, K.Z. ELwakeel, Adsorption behaviour of non-transition metal ions on a synthetic chelating resin bearing iminoacetate function, Sep. Purif. Technol., 43 (2005) 43–48.
[19] H. Zhou, H.X. Zhu, F. Xue, H. Hui, S.F. Wang, Cellulose-based amphoteric adsorbent for the complete removal of low-level heavy metal ions via a specialization and cooperation mechanism, Chem. Eng. J., 385 (2020) 123879, doi: 10.1016/j.cej.2019.123879.
[20] C.-Z. Zhang, H. Sheng, Y.-X. Su, J.-Q. Xu, An efficient and health-friendly adsorbent N-[4-morpholinecarboximidamidoyl] carboximidamidoylmethylated polyphenylene sulfide for removing heavy metal ions from water, J. Mol. Liq., 296 (2019) 111860, doi: 10.1016/j.molliq.2019.111860.
[21] V. Nejadshafiee, M. Reza Islami, Adsorption capacity of heavy metal ions using sultone-modified magnetic activated carbon as a bio-adsorbent, Mater. Sci. Eng., C, 101 (2019) 42–52.
[22] D. Kołodyńska, D. Fila, Z. Hubicki, Evaluation of possible use of the macroporous ion exchanger in the adsorption process of rare earth elements and heavy metal ions from spent batteries solutions, Chem. Eng. Process. Process Intensif., 147 (2020) 107767, doi: 10.1016/j.cep.2019.107767.
[23] K. Kaur, R. Jindal, Synergistic effect of organic-inorganic hybrid nanocomposite ion exchanger on photocatalytic degradation of Rhodamine-B dye and heavy metal ion removal from industrial effluents, J. Environ. Chem. Eng., 6 (2018) 7091–7101.
[24] J.C. Ma, J.W. Shen, C.Z. Wang, Y.M. Wei, Preparation of dual-function chelating resin with high capacity and adjustable adsorption selectivity to variety of heavy metal ions, J. Taiwan Inst. Chem. Eng., 91 (2018) 532–538.
[25] B. Feist, R. Sitko, Fast and sensitive determination of heavy metal ions as batophenanthroline chelates in food and water samples after dispersive micro-solid phase extraction using graphene oxide as sorbent, Microchem. J., 147 (2019) 30–36.
[26] M. Cegłowski, B. Gierczyk, M. Frankowski, Ł. Popenda, A new low-cost polymeric adsorbents with polyamine chelating groups for efficient removal of heavy metal ions from water solutions, React. Funct. Polym., 131 (2018) 64–74.
[27] O. Tavakoli, V. Goodarzi, M.S. Reza, N.M. Mohammad, R. Borja, Competitive removal of heavy metal ions from squid oil under isothermal condition by CR11 chelate ion exchanger, J. Hazard. Mater., 334 (2017) 256–266.
[28] H. Chen, Y. Zhao, Q.Y. Yang, Q. Yan, Preparation of poly-ammonium/sodium dithiocarbamate for the efficient removal of chelated heavy metal ions from aqueous environments, J. Environ. Chem. Eng., 6 (2018) 2344–2354.
[29] S. Lapwanit, T. Trakulsujaritchok, P.N. Nongkhai, Chelating magnetic copolymer composite modified by click reaction for removal of heavy metal ions from aqueous solution, Chem. Eng. J., 289 (2016) 286–295.
[30] C.S. Li, X.X. Li, Y. Liu, Y. Sun, Implications from the grafting density and ionic capacity effects on protein adsorption to poly(N,N-dimethylaminopropyl acrylamide)-grafted sepharose FF, Biochem. Eng. J., 157 (2020) 107546, doi: 10.1016/j.bej.2020.107546.
[31] M. Edwin, P. Sadanand, R. James, Microwave-assisted green synthesis of xanthan gum grafted diethylamino ethyl methacrylate: an efficient adsorption of hexavalent chromium, Carbohydr. Polym., 222 (2019) 114989, doi: 10.1016/j.carbpol.2019.114989.
[32] L.S. Kostenko, I.I. Tomashchuk, T.V. Kovalchuk, O.A. Zaporozhets, Bentonites with grafted aminogroups: synthesis, protolytic properties and assessing Cu(II), Cd(II) and Pb(II) adsorption capacity, Appl. Clay Sci., 172 (2019) 49–56.
[33] E. Gicquel, C. Martin, L. Heux, B. Jean, J. Bras, Adsorption versus grafting of poly(N-Isopropylacrylamide) in aqueous conditions on the surface of cellulose nanocrystals, Carbohydr. Polym., 210 (2019) 100–109.
[34] J.J. Wang, J. Wei, J. Li, Straw-supported ion imprinted polymer sorbent prepared by surface imprinting technique combined with AGET ATRP for selective adsorption of La^{3+} ions, Chem. Eng. J., 293 (2016) 24–33.
[35] K. Khezri, Y. Fazli, Evaluation of the effect of hydrophobically modified silica aerogel on the ARGET ATRP of styrene and butyl acrylate, Microporous Mesoporous Mater., 280 (2019) 236–242.
[36] A. Gopinath, N.A. Sultan, Fluorescent star ATRP initiators and fluorescent star poly(methyl methacrylate)s: synthesis and photophysical properties, Polymer, 153 (2018) 139–149.
[37] Y.N. Chen, W. Zhao, H. Wang, Y.H. Li, C.X. Li, Preparation of novel polyamine-type chelating resin with hyperbranched structures and its adsorption performance, R. Soc. Open Sci., 5 (2018) 171665, doi: 10.1098/rsos.171665.
[38] A.O. Dada, F.A. Adekola, E.O. Odebunmi, F.E. Dada, O.M. Bello, B.A. Akinyemi, O.S. Bello, O.G. Umukoro, Sustainable and low-cost *Ocimum gratissimum* for biosorption of indigo carmine dye: kinetics, isotherm, and thermodynamic studies, Int. J. Phytorem., 22 (2020) 1524–1537.
[39] A.O. Dada, F.A. Adekola, E.O. Odebunmi, A novel zerovalent manganese for removal of copper ions: synthesis, characterization and adsorption studies, Appl. Water Sci., 7 (2015) 1409–1427.
[40] M.O. Olakunle, A.A. Inyinbor, A.O. Dada, O.S. Bello, Combating dye pollution using cocoa pod husks: a sustainable approach, Int. J. Sustainable Eng., 11 (2018) 4–15.
[41] A.L. Wang, Y. Si, H.B. Yin, J. Chen, J.C. Huo, Synthesis of Na-, Fe-, and Mg-containing titanate nanocomposites starting from ilmenite and NaOH and adsorption kinetics, isotherms, and thermodynamics of Cu(II), Cd(II), and Pb(II) cations, Mater. Sci. Eng., B, 249 (2019) 114411, doi: 10.1016/j.mseb.2019.114411.
[42] M.Y. Abdelnaeim, I.Y. El-Sherif, A.A. Attia, N.A. Fathy, M.F. El-Shahat, Impact of chemical activation on the adsorption performance of common reed towards Cu(II) and Cd(II), Int. J. Miner. Process., 157 (2016) 80–88.
[43] Q.Z. Zhou, B.H. Liao, L.N. Lin, W.W. Qiu, Z.G. Song, Adsorption of Cu(II) and Cd(II) from aqueous solutions by ferromanganese

binary oxide–biochar composites, Sci. Total Environ., 615 (2018) 115–122.
[44] J.H. Qu, X. Tian, Z. Jiang, B. Cao, M.S. Akindolie, Q. Hu, C.C. Feng, Y. Feng, X.L. Meng, Y. Zhang, Multi-component adsorption of Pb(II), Cd(II) and Ni(II) onto microwave-functionalized cellulose: kinetics, isotherms, thermodynamics, mechanisms and application for electroplating wastewater purification, J. Hazard. Mater., 387 (2020) 121718, doi: 10.1016/j.jhazmat.2019.121718.
[45] Y.-X. Ma, W.-J. Shao, W. Sun, Y.-L. Kou, X. Li, H.-P. Yang, One-step fabrication of β-cyclodextrin modified magnetic graphene oxide nanohybrids for adsorption of Pb(II), Cu(II) and methylene blue in aqueous solutions, Appl. Surf. Sci., 459 (2018) 544–553.
[46] A. de O. Jorgetto, A.C.P. Silva, M.H.P. Wondracek, R.I.V. Silva, E.D. Velini, M.J. Saeki, V.A. Pedrosa, G.R. Castro, Multilayer adsorption of Cu(II) and Cd(II) over Brazilian Orchid Tree (*Pata-de-vaca*) and its adsorptive properties, Appl. Surf. Sci., 345 (2015) 81–89.